$YZ\beta$ Discontinuity Capturing for Advection-Dominated Processes with Application to Arterial Drug Delivery

Y. Bazilevs [a,1], V.M. Calo [a,1], T.E. Tezduyar [b,2], and T.J.R. Hughes [a,3]

[a] *Institute for Computational Engineering and Sciences, The University of Texas at Austin, 201 East 24th Street, 1 University Station C0200, Austin, TX 78712, USA*

[b] *Mechanical Engineering, Rice University - MS 321, 6100 Main Street, Houston, TX 77005, USA*

Abstract

The $YZ\beta$ discontinuity-capturing operator, recently introduced in [30] in the context of compressible flows, is applied to a time-dependent, scalar advection-diffusion equation with the purpose of modeling drug delivery processes in blood vessels. The formulation is recast in a residual-based form, which reduces to the previously proposed formulation in the limit of zero diffusion and source term. The NURBS-based Isogeometric Analysis method, proposed by Hughes *et al.* [23], was used for the numerical tests. Effects of various parameters in the definition of the $YZ\beta$ operator are examined on a model problem and the better performer is singled out. While for low-order B-spline functions discontinuity capturing is necessary to improve solution quality, we find that high-order, high-continuity B-spline discretizations produce sharp, nearly monotone layers without the aid of discontinuity capturing. Finally, we successfully apply the $YZ\beta$ approach to the simulation of drug delivery in patient-specific coronary arteries.

Key words: discontinuity capturing, fluids, isogeometric analysis, advection-diffusion equation, interior layers, Navier–Stokes equations, drug delivery

[1] Postdoctoral Fellow

[2] James F. Babour Professor of Mechanical Engineering and Materials Sciences

[3] Professor of Aerospace Engineering and Engineering Mechanics, Computational and Applied Mathematics Chair III

1 Introduction

In order to treat coronary artery disease, it has been proposed to deliver drugs to the diseased region of the arterial wall. One such method of delivery is direct injection of the drug into the blood stream in hope that it would reach and penetrate into the arterial wall at a desired location. In order to make the procedure effective, that is, to deliver the necessary amount of the drug to the region of interest with minimal interference with the vascular system, one needs to optimize quantities such as the location of the injector, the injection rate, and the angle of injection. These optimizations can be performed by employing numerical simulation.

A simplified mathematical model that describes the behavior of the drug in the blood stream is a time-dependent, scalar advection-diffusion equation. The scalar in the formulation represents the drug concentration in the blood. The advective velocity for the scalar is assumed to be the blood velocity. In this work we model the blood as an incompressible Newtonian fluid. It is also assumed that the drug concentration does not influence the flow physics. As a result, we have a one-way coupling, in which we first solve for the blood velocity and pressure, and then use the flow field to obtain the drug concentration. Drug dispersivity is assumed very small (yet non-negligible), implying that advective processes take place on a much faster time scale than drug dispersion. It needs to be emphasized that in the advective-diffusive model employed herein the drug cannot reach the wall without dispersion.

With the above assumptions, the transport equation models nearly pure advection phenomena that, for practical meshes, leads to unresolved interior and boundary layers, which, in turn, pose a challenge for most existing numerical techniques. Oscillations are typically seen in the vicinities of the layers. It is generally accepted that SUPG stabilization (see [7]) is not sufficiently dissipative in the vicinity of sharp gradients to preclude significant undershoots and overshoots in the discrete solution. Discontinuity capturing, also referred to as shock capturing, provides further dissipation and improves the quality of the discrete solution near sharp layers. Discontinuity-capturing operators are designed to be active in the region of high solution gradients and vanish quickly in the parts of the domain where the solution is smooth.

The paper is outlined as follows. In Section 2, we describe the strong and weak formulations of the continuous advection-diffusion problem and then formulate it at the discrete level. We employ SUPG stabilization augmented by a $YZ\beta$ discontinuity-capturing operator, which was originally proposed by Tezduyar in [30] in the context of compressible flows, and was shown in [34–36] to produce results superior to existing formulations. We extend the original $YZ\beta$ definition to the scalar advection-diffusion case and rewrite it in the residual-based form. The rest of the paper is devoted to various numerical test cases. In all examples spatial discretiza-

tion makes use of the NURBS-based Isogeometric Analysis approach (see [4, 12, 23]). Time integration is performed using the Generalized-α method (see [10, 25]).

In Section 3, we consider a numerical example that deals with advection of an L-shaped discontinuity front. We focus on the performance of the method in the transient regime and compare solutions with and without discontinuity capturing. We also investigate the effects of the "advective" versus the residual-based forms of the $YZ\beta$ operator. For second-order, C^1-continuous B-spline discretization we find that residual-based formulations produce sharper discontinuities without significant over- and under-shooting, and are less sensitive to the variations of the sharpness parameter β used in the definition of $YZ\beta$. By solving the same problem on the mesh of sixth-order B-splines that are C^5-continuous, we also find that high-order, high-continuity discretizations produce excellent quality layers without the aid of discontinuity capturing. This result confirms the findings of Hughes *et al.* [23] for steady advection-diffusion problems. In Section 4, we apply the $YZ\beta$ formulation of the advection-diffusion equation to model drug delivery in patient-specific coronary arteries. Second-order NURBS are employed in this example (for details of patient-specific NURBS geometry construction for use in isogeometric analysis, see [37]). In Section 5 we draw conclusions and outline future research directions.

2 Advection-Diffusion Equation

2.1 Strong and weak formulations of the continuous problem

Let Ω be an open, connected, bounded subset of $\mathbb{R}^d$, $d = 2$ or 3, with piecewise smooth boundary $\Gamma = \partial\Omega$. Ω represents the fixed spatial domain of the problem. Let $f : \Omega \to \mathbb{R}$ be the given source; $\boldsymbol{a} : \Omega \to \mathbb{R}^d$ is the spatially varying velocity vector, assumed solenoidal; and $\boldsymbol{\kappa} : \Omega \to \mathbb{R}^{d\times d}$ is the diffusivity tensor, assumed symmetric, positive-definite. The boundary value problem consists of solving the following equations for $\phi : \overline{\Omega} \to \mathbb{R}$:

$$\mathcal{L}\phi = f \quad \text{in } \Omega, \tag{1}$$

$$\phi = g \quad \text{on } \Gamma_D, \tag{2}$$

$$\boldsymbol{\kappa}\nabla\phi \cdot \boldsymbol{n} = h \quad \text{on } \Gamma_N, \tag{3}$$

where

$$\mathcal{L}\phi = \frac{\partial\phi}{\partial t} + \boldsymbol{a} \cdot \nabla\phi - \nabla \cdot (\boldsymbol{\kappa}\nabla\phi), \tag{4}$$

and $g : \Gamma_D \to \mathbb{R}$ is the prescribed Dirichlet boundary data, $h : \Gamma_N \to \mathbb{R}$ is the prescribed Neumann boundary data, $\boldsymbol{n}$ is the unit outward boundary normal, $\Gamma = \Gamma_D \cup \Gamma_N$, and $\Gamma_D \cap \Gamma_N = \emptyset$.

Defining the solution and the weighting function spaces as

$$H^1_g(\Omega) = \{\phi \mid \phi \in H^1(\Omega),\ \ \phi = g \ \ \text{on}\ \Gamma\}, \tag{5}$$
$$H^1_0(\Omega) = \{\phi \mid \phi \in H^1(\Omega),\ \ \phi = 0 \ \ \text{on}\ \Gamma\}, \tag{6}$$

respectively, the variational counterpart of (1) reads: Find $\phi \in H^1_g(\Omega)$ such that $\forall w \in H^1_0(\Omega)$,

$$(w, \frac{\partial \phi}{\partial t} + \boldsymbol{a} \cdot \nabla \phi)_\Omega + (\nabla w, \boldsymbol{\kappa} \nabla u)_\Omega = (w, f)_\Omega + (w, h)_{\Gamma_N}, \tag{7}$$

where $(\cdot, \cdot)_A$ denotes the L^2-inner product on $A = \{\Omega, \Gamma\}$.

2.2 Discrete formulation and discontinuity-capturing

Let $\mathcal{V}^h_g$ and $\mathcal{V}^h_0$ be the finite-dimensional spaces of trial solutions and weighting functions, respectively, where, as in the continuous case, subscripts g and 0 refer to essential boundary conditions. We state the semi-discrete formulation of the advection-diffusion problem as follows: Find $\phi^h \in \mathcal{V}^h_g$ such that $\forall w^h \in \mathcal{V}^h_0$,

$$\begin{aligned}(w^h, \frac{\partial \phi^h}{\partial t} + \boldsymbol{a} \cdot \nabla \phi^h)_\Omega + (\nabla w^h, \boldsymbol{\kappa} \nabla \phi^h)_\Omega - (w^h, f)_\Omega - (w^h, h)_{\Gamma_N} \\ + \sum_{e=1}^{n_{el}} (\boldsymbol{a} \cdot \nabla w^h \tau, \mathcal{L}\phi^h - f)_{\Omega_e} + (\nabla w^h, \boldsymbol{\kappa}_{dc} \nabla \phi^h)_{\Omega_e} = 0.\end{aligned} \tag{8}$$

In this work we make use of the spaces of NURBS functions employed in isogeometric analysis [23]. The developments that follow are equally applicable to standard finite element discretizations. The above formulation of advection-diffusion makes use of SUPG stabilization, in which

$$\tau = \frac{h_{\boldsymbol{a}}}{2|\boldsymbol{a}|} \min(1, \frac{1}{3p^2} Pe), \tag{9}$$

where Pe, the element Peclet number, is defined as

$$Pe = \frac{|\boldsymbol{a}| h_{\boldsymbol{a}}}{2|\boldsymbol{\kappa}|}, \tag{10}$$

$h_{\boldsymbol{a}}$ is the element size in the direction of the flow, and p is the polynomial order of the basis. For a summary of the early literature on the SUPG formulation see Brooks and Hughes [7]. Recent work on stabilized methods is presented in [1, 5, 6, 8, 11, 13–16, 27, 28, 31–33]. The definition of the intrinsic time scale τ, given by (9), is adequate for simple element geometries. It is based on a single, advective length scale, $h_{\boldsymbol{a}}$. A more general definition, which involves a single, diffusive length scale, is given and utilized in the description of the drug delivery computations.

Other definitions of τ based on multiple length scales are presented in [32, 33]. The last term of (8) is the discontinuity-capturing operator, and $\boldsymbol{\kappa}_{dc}$ is the associated diffusivity tensor. We make use of the so-called $YZ\beta$ definition of $\boldsymbol{\kappa}_{dc}$ introduced in [30] for compressible flows. In this work we start by extending that formulation to the unsteady, scalar advection-diffusion equation.

The discontinuity-capturing diffusion tensor $\boldsymbol{\kappa}_{dc}$ is defined as

$$\boldsymbol{\kappa}_{dc} = \kappa_{dc}\boldsymbol{D}, \tag{11}$$

where κ_{dc} is the magnitude and $\boldsymbol{D}$ defines the direction in which the operator is applied. When $\boldsymbol{D} = \boldsymbol{I}$, the identity tensor, the discontinuity-capturing diffusion is isotropic. Extending the definition of κ_{dc} given in [30, 33] to the scalar case, we get

$$\kappa_{dc} = |Y^{-1}Z|(\sum_{i=1}^{d}|Y^{-1}\frac{\partial\phi^h}{\partial x_i}|^2)^{\beta/2-1}(\frac{h_{dc}}{2})^{\beta}, \tag{12}$$

where

$$Y = \phi_{ref}, \tag{13}$$

is the reference value of the scalar field ϕ^h, and

$$h_{dc} = 2(\sum_{a=1}^{n_{shl}}|\boldsymbol{j}\cdot\nabla N_a|)^{-1}, \tag{14}$$

is the local element length scale. In (14), $\boldsymbol{j} = \frac{\nabla\phi^h}{\|\nabla\phi^h\|}$, N_a is the element basis function, and n_{shl} is the total number of element basis functions. The parameter β in (12) influences the smoothness of the layer. For smoother layers it is set to 1, while for sharper layers it set to 2.

The original $YZ\beta$ is defined in [30, 33] as

$$Z = \boldsymbol{a}\cdot\nabla\phi^h, \tag{15}$$

or

$$Z = \frac{\partial\phi^h}{\partial t} + \boldsymbol{a}\cdot\nabla\phi^h. \tag{16}$$

Expression (15) is applicable to the steady case, while (16) is to be used for time-dependent problems. Note that the original definition is not consistent, namely it does not vanish on the exact solution. In view of this we propose to modify the definition of Z to

$$Z = \mathcal{L}\phi^h - f, \tag{17}$$

In the absence of the source term, and because one typically employs discontinuity-capturing for very small or zero physical diffusion, definition (17) reduces to (15) for the steady problem, and to (16) for the time-dependent case.

In our case, where time-dependent behavior is of interest and diffusion is very small, formulations employing (17) and (16) are, for all practical purposes, equivalent. Numerical examples presented in the next section indicate that omitting the time-derivative term from the definition of Z for time-dependent problems leads to discontinuities that are overly diffuse. This is an important observation, as the computations reported in [34–36] were steady-state computations, and, as a result, employed (15). Furthermore, our numerical experiments show that the choice of the Z term has greater influence on the sharpness of the discontinuity than the parameter β.

3 Tests with an L-Shaped Discontinuity Advected Skew to Mesh

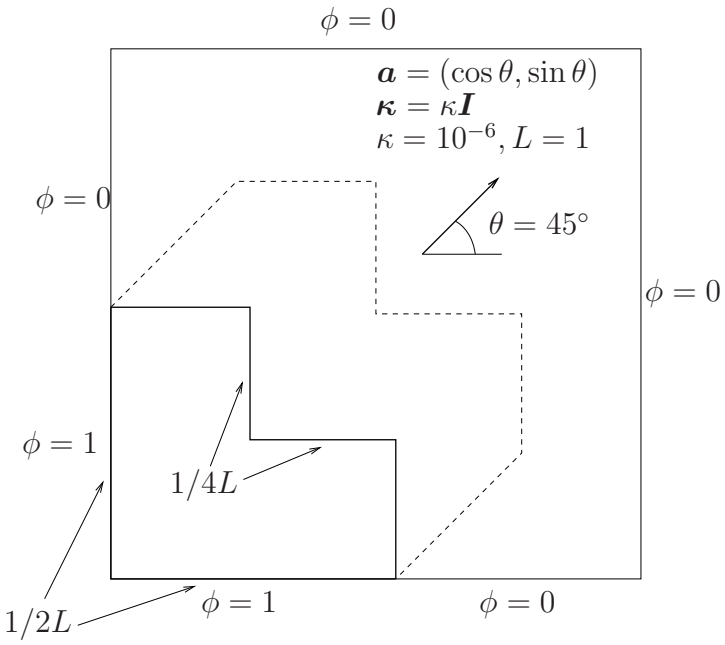

Fig. 1. Advection of an L-shaped front. Problem description.

The problem setup is given in Figure 1. The scalar diffusivity $\boldsymbol{\kappa}$ is assumed isotropic, that is $\boldsymbol{\kappa} = \kappa \boldsymbol{I}$ with $\kappa = 10^{-6}$. The angle of advection is chosen to be $45°$ and the magnitude of the advective speed is set to unity. The domain is a unit square subdivided into 20×20 square elements. At time $t = 0$ the value of the scalar field is set to unity in the interior of the L-shaped block located in the lower left-hand corner of the domain. Elsewhere in the domain ϕ^h is set to zero, creating an interior layer with an L-shaped concave front. We chose this initial shape in order demonstrate robustness and accuracy of the method, since advecting concave surfaces is more challenging than convex ones. The solution is advanced in time until $t = 0.25$.

Given that the diffusion coefficient is very small compared to the advection velocity and the mesh size, for all practical purposes the problem corresponds to pure advection. We will refer to the interior layer as the discontinuity front, and its location and shape at the final time ($t = 0.25$) are illustrated in Figure 1 with dashed lines.

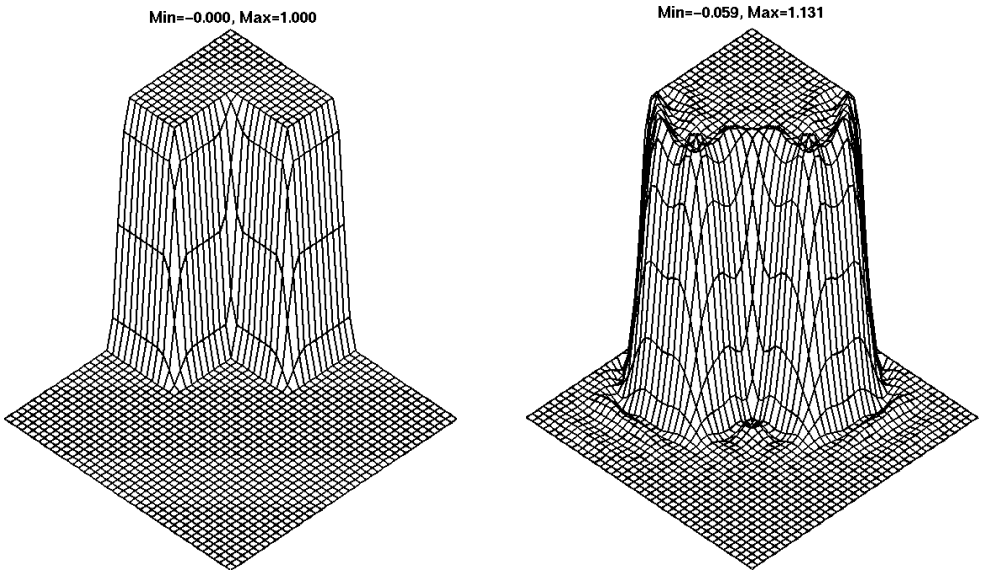

a) Initial condition b) SUPG without discontinuity-capturing

Fig. 2. Advection of an L-shaped front. Results using C^1-continuous quadratic splines. Elevation plot of the solution interpolated with 40×40 bilinear elements.

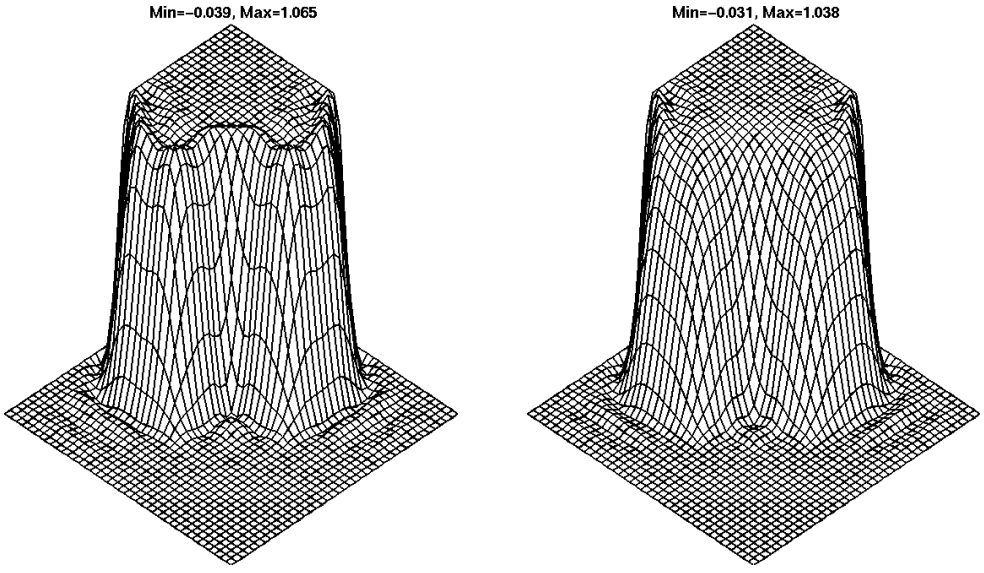

a) Residual-based ($Z = \mathcal{L}\phi^h - f$), $\beta = 2$ b) Advective ($Z = \boldsymbol{a} \cdot \nabla\phi^h$), $\beta = 2$

Fig. 3. Advection of an L-shaped front with discontinuity capturing. Results using C^1-continuous quadratic splines. Elevation plot of the solution interpolated with 40×40 bilinear elements.

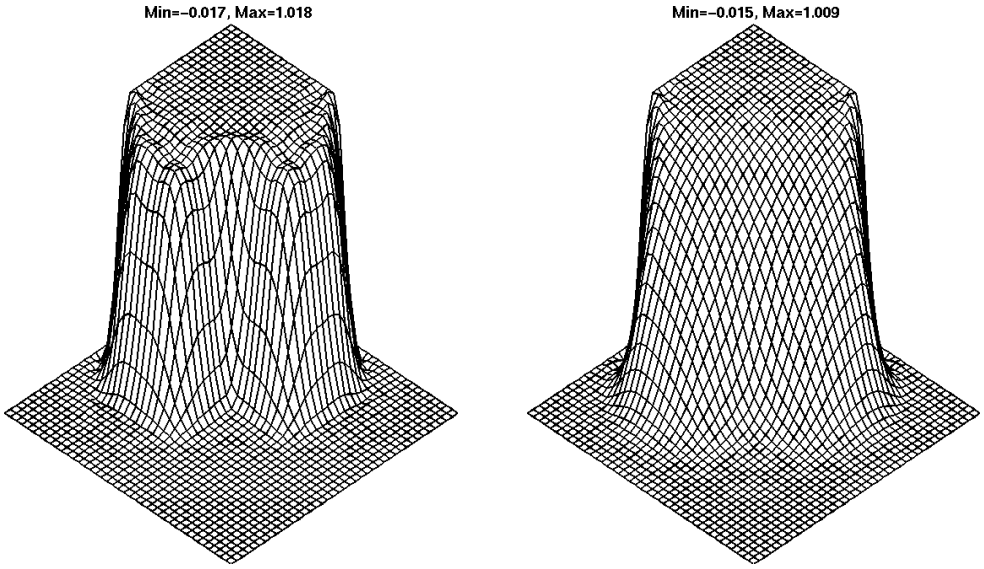

e) Residual-based ($Z = \mathcal{L}\phi^h - f$), $\beta = 1$ f) Advective ($Z = \boldsymbol{a} \cdot \nabla\phi^h$), $\beta = 1$

Fig. 4. Advection of an L-shaped front with discontinuity capturing. Results using C^1-continuous quadratic splines. Elevation plot of the solution interpolated with 40×40 bilinear elements.

Figures 2-4 present results for second-order, C^1-continuous NURBS (B-splines in this case due to the simple geometry). We investigate the $YZ\beta$ discontinuity-capturing operator and test advective ($Z = \boldsymbol{a} \cdot \nabla\phi^h$) versus residual-based ($Z = \mathcal{L}\phi^h - f$) formulations, as well as parameter values $\beta = 1$ and $\beta = 2$. We compare simulation results at $t = 0.25$ in order to examine the ability of a given discrete formulation to generate time-dependent solutions that preserve the sharpness of the discontinuities without excessive undershooting and overshooting. We first note that advective formulations produce significantly more smeared shocks than their residual-based counterparts. We also observe that in the case of the residual-based method the sharpness of the discontinuity is not as strongly dependent on β as for the advective case. Finally, we conclude that for this level of discretization the combination of residual-based formulation and $\beta = 1$ appears to be most favorable.

The next set of results makes use of C^5-continuous B-splines of degree six on the same mesh. It was demonstrated on a particular problem in Hughes *et al.* [23] that high-order, high-continuity discretizations in conjunction with a *linear* stabilized method converge to monotone solutions in the presence of thin layers for steady advection-diffusion. Results of this computation, shown in Figures 5 and 6, indicate that the same behavior is observed for time-dependent advection-diffusion cases. Furthermore, only a slight improvement in the $p = 6$ solution is achieved by using the discontinuity-capturing operator.

It should be noted that boundary conditions for both $p = 2$ and $p = 6$ were set according to the technique described in [23] in which the control variables interpolate the prescribed data. Since the B-spline spaces are non-nested for various polyno-

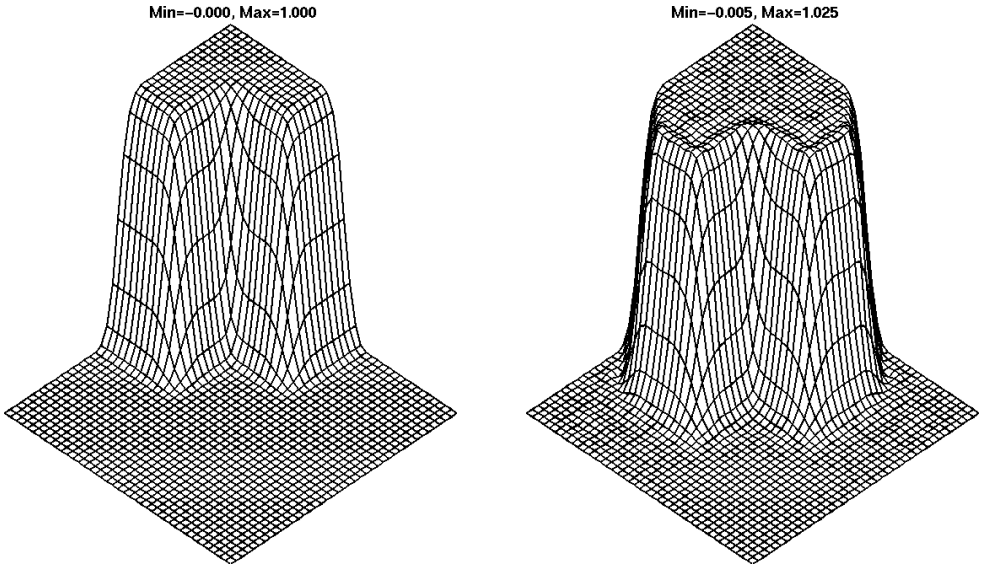

a) Initial condition b) SUPG without discontinuity-capturing

Fig. 5. Advection of an L-shaped front. Results using C^5-continuous splines of order six. Elevation plot of the solution interpolated with 40×40 bilinear elements. Note the sharpness and lack of significant undershoots and overshoots in the SUPG solution without discontinuity capturing.

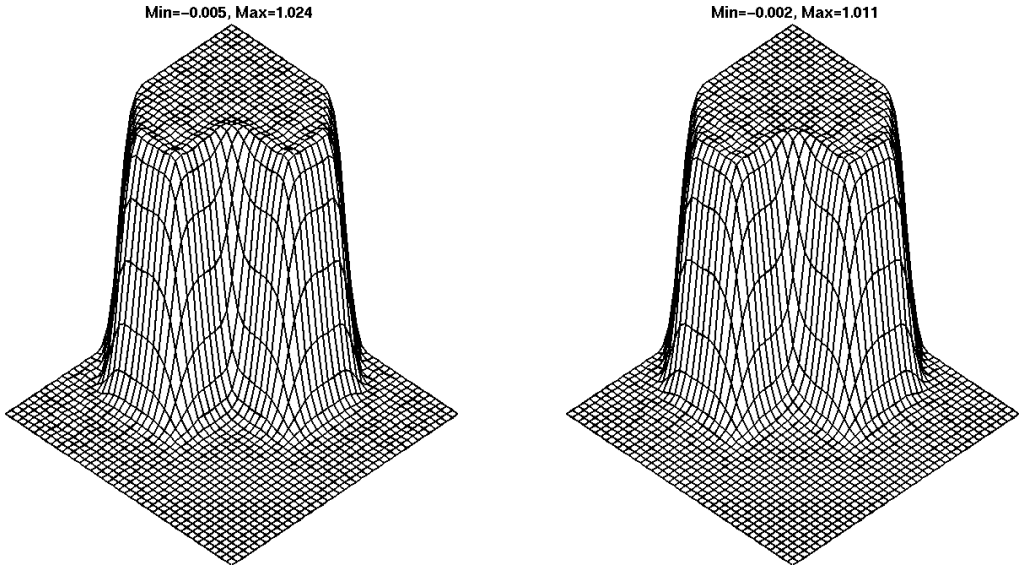

a) Residual-based ($Z = \mathcal{L}\phi^h - f$), $\beta = 2$ b) Residual-based ($Z = \mathcal{L}\phi^h - f$), $\beta = 1$

Fig. 6. Advection of an L-shaped front with discontinuity capturing. Results using C^5-continuous splines of order six. Elevation plot of the solution interpolated with 40×40 bilinear elements.

mial orders, the boundary conditions are slightly different for both cases, the $p = 6$ case being somewhat more smeared due to the greater support of the basis functions (see Figures 2a and 5a for a comparison).

4 Patient-Specific Modeling of Drug Delivery in Coronary Arteries

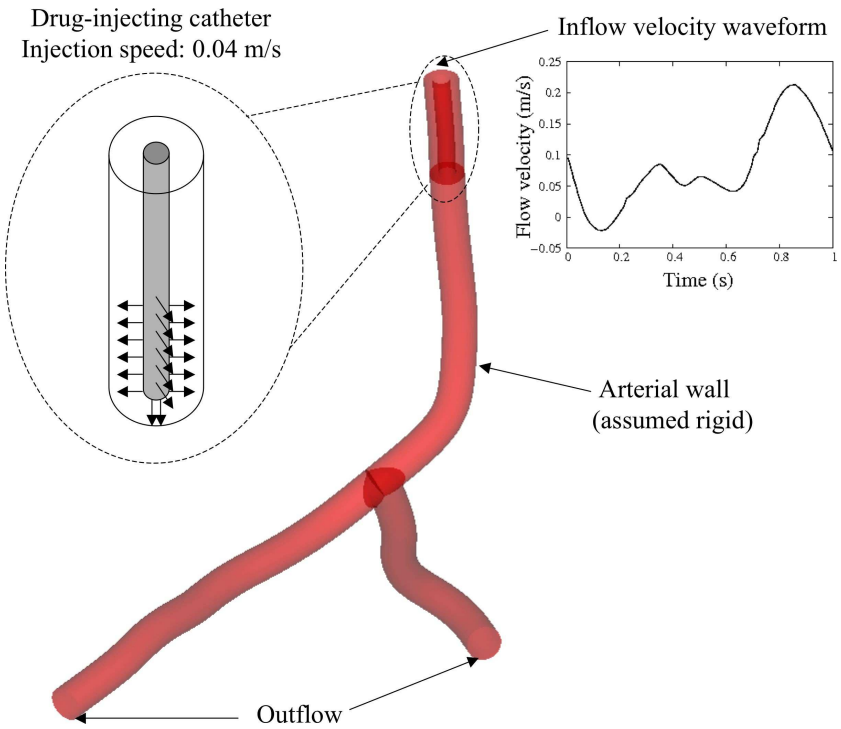

Fig. 7. Patient-specific modeling of drug delivery in coronary arteries. Problem setup. The inflow data was takes from [26, 29].

In this computational study we have developed a model, which makes use of patient-specific geometry of a portion of the coronary arterial tree of a healthy over 55 volunteer obtained from 64-slice CT angiography. The setup for this study is illustrated in Figure 7. At the inlet of the artery we have placed a nearly cylindrical catheter for the purposes of injecting the drug into the blood stream. Blood is described as an incompressible Newtonian fluid with density of 1.06 g/cm^3 and viscosity of 0.035 g/(cm s). A periodic flow waveform is applied at the inlet with a period of 1 s. The catheter is assumed to inject the drug into the flow at the speed of 4 cm/s in the direction normal to its lateral surface. It is also assumed that the drug is injected from the bottom half of the catheter and its tip, as indicated in Figure 7. Prior to the drug being released, a fully periodic flow solution was attained. The drug is released in the beginning of a period and it is injected at a constant velocity thereafter.

The evolution of the drug concentration in the bloodstream is assumed to be governed by a time-dependent advection-diffusion equation with ϕ representing the concentration value. The advection velocity is assumed to come from the solution of the Navier-Stokes equations. It is also assumed that the drug concentration does not influence the flow physics, hence we have a one-way coupling. The drug diffusivity tensor $\boldsymbol{\kappa}$ is assumed to be isotropic and constant with κ taken to be 0.35×10^{-6} cm^2/s. Boundary conditions for the drug concentration are as follows:

on the catheter, where the injection velocity is nonzero, the drug concentration is set to one, while on the rest of the catheter, as well as at the inflow, the drug concentration is set to zero. Arterial walls and outflow boundaries are assigned a homogeneous Neumann boundary condition.

Isogeometric analysis employing quadratic NURBS is used for the spatial disctetization. The arterial wall is assumed rigid in the computations, as the focus is placed on the advection-diffusion formulation rather than on the fluid-structure interaction. Future work will entail extending the drug delivery formulation to fluid-structure interaction with a poroelastic arterial wall. Applications of NURBS-based isogeometric analysis to fluid-structure interaction in arterial blood flow, where the arterial wall is assumed deformable, can be found in [3, 37].

A residual-based multiscale method (see e.g., [2, 9, 22]), founded on the variational multiscale formulation of the Navier-Stokes equations of incompressible flows (see e.g., [17–21, 24]), is used for the fluid mechanics part. These residual-based methods possess a dual nature: on the one hand they are bona-fide LES-like turbulence models, and on the other hand they may be thought of as stabilized methods, such as the SUPG formulation, extended to the nonlinear realm and capable of accurately solving laminar flows. For the scalar advection-diffusion equation we use the $YZ\beta$ discontinuity-capturing formulation with $\beta = 1$. For this case we use a definition of τ that is different from (9) and that is more suitable for complex element geometries

$$\tau = (4/\Delta t^2 + \boldsymbol{a} \cdot \boldsymbol{G}\boldsymbol{a} + 9p^4\nu^2 \boldsymbol{G} : \boldsymbol{G})^{-1/2}, \tag{18}$$

where $\boldsymbol{G}$ is a second-rank metric tensor

$$\boldsymbol{G} = \left(\frac{\partial \boldsymbol{\xi}}{\partial \boldsymbol{x}}\right)^T \frac{\partial \boldsymbol{\xi}}{\partial \boldsymbol{x}}, \tag{19}$$

$\frac{\partial \boldsymbol{\xi}}{\partial \boldsymbol{x}}$ is the inverse Jacobian of the element mapping between the parent and the physical domain, and Δt is the time step.

Figure 8 shows snapshots of the drug concentration in the interior of the coronary artery at $t = 0.2$ s and $t = 0.8$ s during four heartbeat cycles. Note that no significant overshoots and undershoots in the solution are present. Also note the quality of the sharp layers, which does not degrade as the scalar is advanced in time for several heartbeat cycles. This is due to the superior robustness of the $YZ\beta$ discontinuity-capturing scheme. The longer the drug is injected into the blood stream, the more it is deposited on the arterial walls. This effect can be seen in Figure 9. Also note that at $t = 0.2$ s, at which time the inflow waveform is approximately zero (see insert in Figure 7), most of the inflow volume comes from the catheter, which results in increased drug concentration at the wall immediately near the catheter, since the drug is injected normal to the streamwise direction. On the other hand, at $t = 0.8$ s, most of the flow goes in the stream-wise direction, carrying the drug with it and

depositing very little on the wall adjacent to the catheter. Figures 8 and 9 clearly demonstrate this feature.

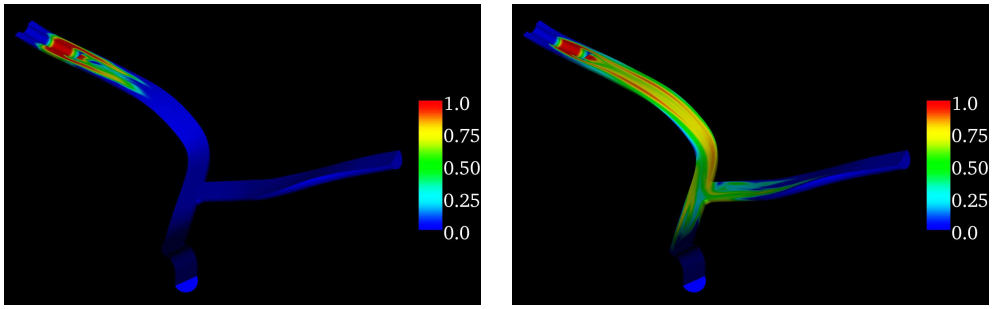

a) Cycle one, $t = 0.2$ s

b) Cycle one, $t = 0.8$ s

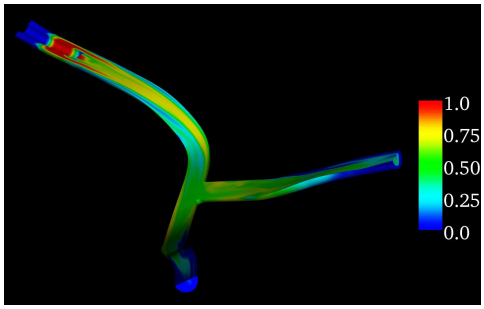

c) Cycle two, $t = 0.2$ s

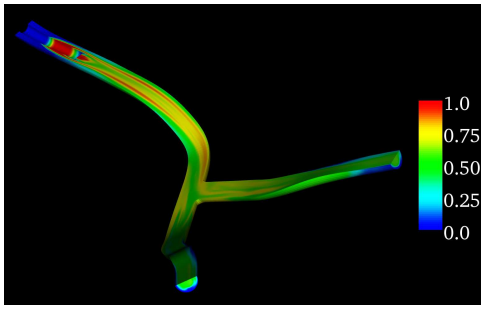

d) Cycle two, $t = 0.8$ s

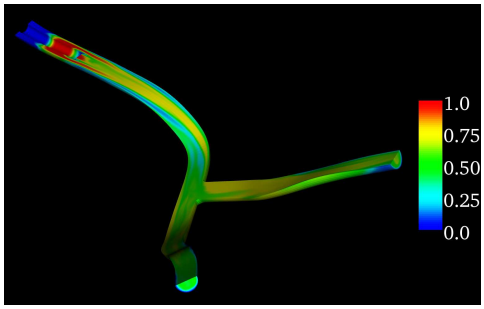

e) Cycle three, $t = 0.2$ s

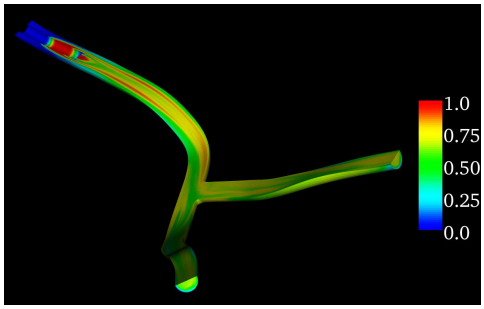

f) Cycle three, $t = 0.8$ s

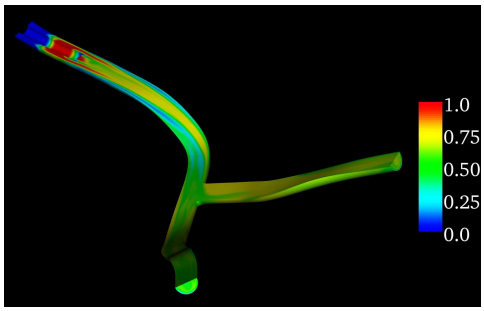

g) Cycle four, $t = 0.2$ s

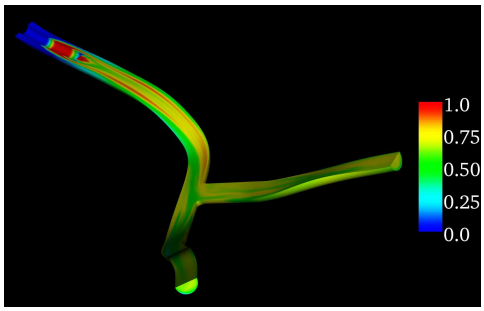

h) Cycle four, $t = 0.8$ s

Fig. 8. Patient-specific modeling of drug delivery in coronary arteries. Drug concentration in the interior of the arteries at various instants during the simulation.

In all cases, the highest drug concentration at the wall is achieved in the region where the artery bifurcates. It is also at the bifurcation that the flow is most three-dimensional, containing complex structures, such as swirling and recirculation. This indicates that the drug is more likely to be deposited on the artery wall where the flow is most unsteady. A detailed view of the bifurcation area is shown in Figure 10, from which we observe that by the fourth heart cycle both the fluid and the drug solutions become nearly time-periodic.

5 Conclusions

We have extended the $YZ\beta$ formulation to the time-dependent, scalar advection-diffusion equation and recast it in a residual-based form. Using a simple test case we demonstrated that the inclusion of the time-dependent part of the differential operator in the definition of Z is important in order to produce sharp interior layers without excessive overshooting and undershooting. We also found that the residual-based formulation exhibits weaker dependence on the sharpness parameter β than its advective counterpart. In the case of splines of high-order and high-continuity, the SUPG formulation without the aid of discontinuity capturing produced very good interior layers.

We have successfully applied the $YZ\beta$ formulation to patient-specific modeling of drug delivery in coronary arteries. We have observed that the formulation is capable of preserving sharp features of the solution for several heartbeat cycles without degrading quality, exhibiting a high level of robustness necessary for real-world applications. A more extensive exploration of drug delivery in arteries is in progress.

While stabilized methods may be derived on the basis of the variational multiscale methodology, discontinuity-capturing is an ad hoc technique. Nevertheless, it is a widely used technology that enables a practitioner to successfully tackle real-world applications. We believe that the multiscale framework with a proper set of optimality conditions is the right underlying theoretical structure that may more naturally lead to discontinuity-capturing formulations. This conjecture is intriguing and warrants further investigation.

Acknowledgements

Y. Bazilevs was partially supported by the J.T. Oden ICES Postdoctoral Fellowship at the Institute for Computational Engineering and Sciences (ICES). This support is gratefully acknowledged. We would also like to thank Y. Zhang of ICES for providing us with geometry data for coronary arteries, as well as G. Johnson at

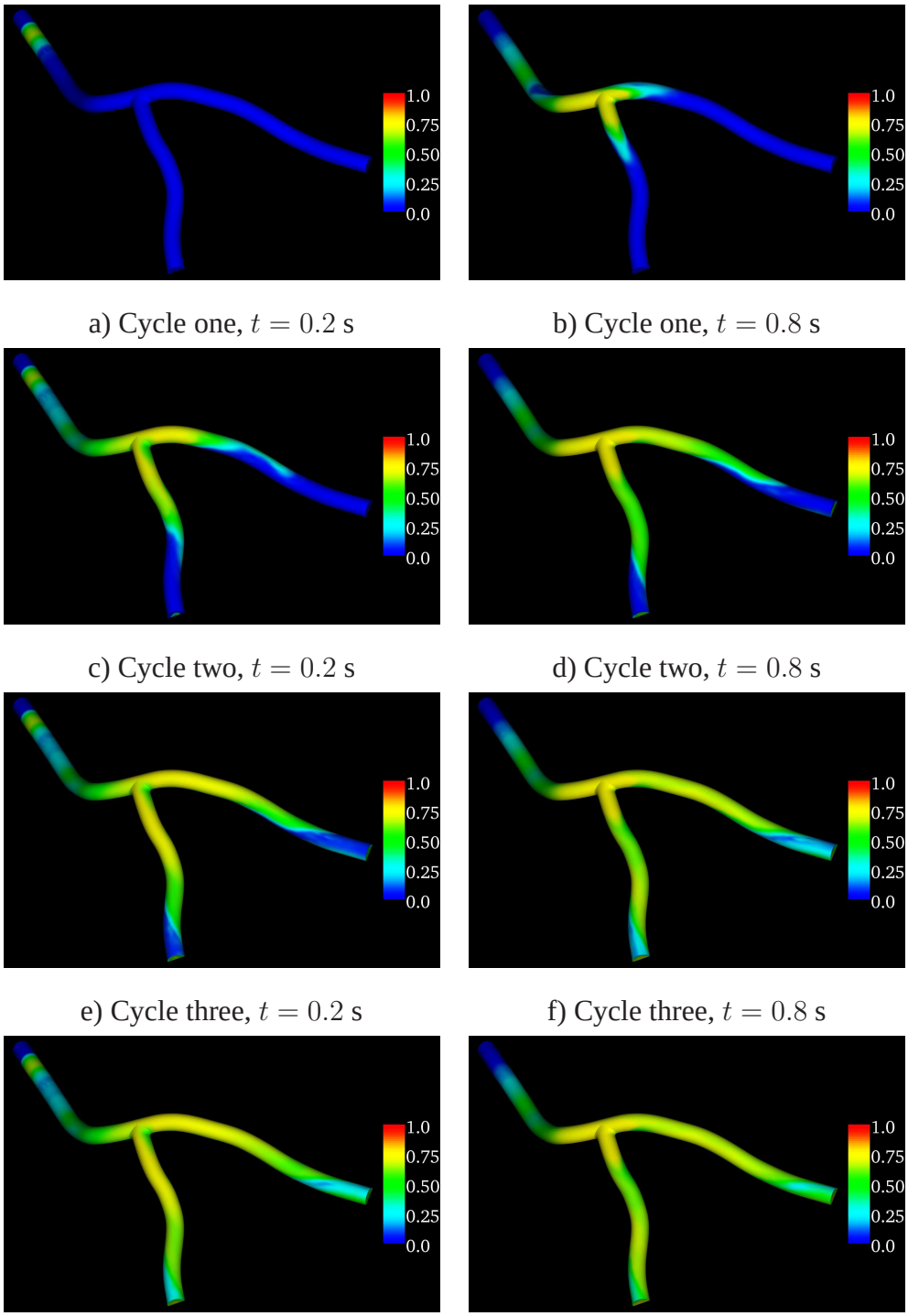

a) Cycle one, $t = 0.2$ s

b) Cycle one, $t = 0.8$ s

c) Cycle two, $t = 0.2$ s

d) Cycle two, $t = 0.8$ s

e) Cycle three, $t = 0.2$ s

f) Cycle three, $t = 0.8$ s

g) Cycle four, $t = 0.2$ s

h) Cycle four, $t = 0.8$ s

Fig. 9. Patient-specific modeling of drug delivery in coronary arteries. Drug concentration at the arterial wall at various instants during the simulation.

the Texas Advanced Computing Center for helping us with visualization of arterial blood flow. This study was partially supported by Abbott Vascular Contract No. UTA06-520 and Texas ARP (Advanced Research Program) Grant No. ARP-

003658-0025-2006-Hughes.

References

[1] J. E. Akin and T. E. Tezduyar. Calculation of the advective limit of the SUPG stabilization parameter for linear and higher-order elements. *Computer Methods in Applied Mechanics and Engineering*, 193:1909–1922, 2004.

[2] Y. Bazilevs. *Isogeometric Analysis of Turbulence and Fluid-Structure Interaction*. PhD thesis, ICES, UT Austin, 2006.

[3] Y. Bazilevs, V. M. Calo, Y. Zhang, and T. J. R. Hughes. Isogeometric fluid-structure interaction analysis with applications to arterial blood flow. *Computational Mechanics*, 38:310–322, 2006.

[4] Y. Bazilevs, L. Beirao da Veiga, J.A. Cottrell, T.J.R. Hughes, and G. Sangalli. Isogeometric analysis: Approximation, stability and error estimates for h-refined meshes. *Mathematical Models and Methods in Applied Sciences*, 16:1031–1090, 2006.

[5] M. Bischoff and K.-U. Bletzinger. Improving stability and accuracy of Reissner-Mindlin plate finite elements via algebraic subgrid scale stabilization. *Computer Methods in Applied Mechanics and Engineering*, 193:1491–1516, 2004.

[6] P. B. Bochev, M. D. Gunzburger, and J. N. Shadid. On inf-sup stabilized finite element methods for transient problems. *Computer Methods in Applied Mechanics and Engineering*, 193:1471–1489, 2004.

[7] A. N. Brooks and T. J. R. Hughes. Streamline upwind / Petrov-Galerkin formulations for convection dominated flows with particular emphasis on the incompressible Navier-Stokes equations. *Computer Methods in Applied Mechanics and Engineering*, 32:199–259, 1982.

[8] E. Burman and P. Hansbo. Edge stabilization for Galerkin approximations of convection-diffusion-reaction problems. *Computer Methods in Applied Mechanics and Engineering*, 193:1437–1453, 2004.

[9] V.M. Calo. *Residual-based Multiscale Turbulence Modeling: Finite Volume Simulation of Bypass Transistion*. PhD thesis, Department of Civil and Environmental Engineering, Stanford University, 2004.

[10] J. Chung and G. M. Hulbert. A time integration algorithm for structural dynamics with improved numerical dissipation: The generalized-α method. *Journal of Applied Mechanics*, 60:371–75, 1993.

[11] R. Codina and O. Soto. Approximation of the incompressible Navier-Stokes equations using orthogonal subscale stabilization and pressure segregation on anisotropic finite element meshes. *Computer Methods in Applied Mechanics and Engineering*, 193:1403–1419, 2004.

[12] J.A. Cottrell, A. Reali, Y. Bazilevs, and T.J.R. Hughes. Isogeometric analysis of structural vibrations. *Computer Methods in Applied Mechanics and Engineering*, 195:5257–5297, 2006.

[13] A. L. G. A. Coutinho, C. M. Diaz, J. L. D. Alvez, L. Landau, A. F. D. Loula, S. M. C. Malta, R. G. S. Castro, and E. L. M. Garcia. Stabilized methods and post-processing techniques for miscible displacements. *Computer Methods in Applied Mechanics and Engineering*, 193:1421–1436, 2004.

[14] V. Gravemeier, W. A. Wall, and E. Ramm. A three-level finite element method for the instationary incompressible Navier-Stokes equations. *Computer Methods in Applied Mechanics and Engineering*, 193:1323–1366, 2004.

[15] I. Harari. Stability of semidiscrete formulations for parabolic problems at small time steps. *Computer Methods in Applied Mechanics and Engineering*, 193:1491–1516, 2004.

[16] G. Hauke and L. Valiño. Computing reactive flows with a field Monte Carlo formulation and multi-scale methods. *Computer Methods in Applied Mechanics and Engineering*, 193:1455–1470, 2004.

[17] J. Holmen, T.J.R. Hughes, A.A. Oberai, and G.N. Wells. Sensitivity of the scale partition for variational multiscale LES of channel flow. *Physics of Fluids*, 16(3):824–827, 2004.

[18] T. J. R. Hughes, L. Mazzei, and K. E. Jansen. Large-eddy simulation and the variational multiscale method. *Computing and Visualization in Science*, 3:47–59, 2000.

[19] T. J. R. Hughes, L. Mazzei, A. A. Oberai, and A.A. Wray. The multiscale formulation of large eddy simulation: Decay of homogenous isotropic turbulence. *Physics of Fluids*, 13(2):505–512, 2001.

[20] T. J. R. Hughes, A. A. Oberai, and L. Mazzei. Large-eddy simulation of turbulent channel flows by the variational multiscale method. *Physics of Fluids*, 13(6):1784–1799, 2001.

[21] T. J. R. Hughes, G. Scovazzi, and L. P. Franca. Multiscale and stabilized methods. In E. Stein, R. De Borst, and T. J. R. Hughes, editors, *Encyclopedia of Computational Mechanics, Vol. 3, Computational Fluid Dynamics*, chapter 2. Wiley, 2004.

[22] T.J.R. Hughes, V.M. Calo, and G. Scovazzi. Variational and multiscale methods in turbulence. In W. Gutkowski and T.A. Kowalewski, editors, *In Proceedings of the XXI International Congress of Theoretical and Applied Mechanics (IUTAM)*. Kluwer, 2004.

[23] T.J.R. Hughes, J.A. Cottrell, and Y. Bazilevs. Isogeometric analysis: CAD, finite elements, NURBS, exact geometry, and mesh refinement. *Computer Methods in Applied Mechanics and Engineering*, 194:4135–4195, 2005.

[24] T.J.R. Hughes, G.N. Wells, and A.A. Wray. Energy transfers and spectral eddy viscosity of homogeneous isotropic turbulence: comparison of dynamic Smagorinsky and multiscale models over a range of discretizations. *Physics of Fluids*, 16:4044–4052, 2004.

[25] K. E. Jansen, C. H. Whiting, and G. M. Hulbert. A generalized-α method for integrating the filtered Navier-Stokes equations with a stabilized finite element method. *Computer Methods in Applied Mechanics and Engineering*, 190:305–319, 1999.

[26] B.M. Johnston, P.R. Johnston, S. Corney, and D. Kilpatrick. Non-Newtonian

blood flow in human right coronary arteries: Transient simulation. *Journal of Biomechanics*, 36:1116–1128, 2006.

[27] B. Koobus and C. Farhat. A variational multiscale method for the large eddy simulation of compressible turbulent flows on unstructured meshes – application to vortex shedding. *Computer Methods in Applied Mechanics and Engineering*, 193:1367–1383, 2004.

[28] A. Masud and R. A. Khurram. A multiscale/stabilized finite element method for the advection-diffusion equation. *Computer Methods in Applied Mechanics and Engineering*, 193:1997–2018, 2004.

[29] S. Matsuo, M. Tsuruta, M. Hayano, Y. Immamura, Y. Eguchi, T. Tokushima, and S. Tsuji. Phasic coronary artery flow velocity determined by Doppler flowmeter catheter in aortic stenosis and aortic regurgitation. *The American Journal of Cardiology*, 62:917–922, 1988.

[30] T. E. Tezduyar. Finite element methods for fluid dynamics with moving boundaries and interfaces. In E. Stein, R. De Borst, and T. J. R. Hughes, editors, *Encyclopedia of Computational Mechanics, Vol. 3: Fluids*, chapter 17. Wiley, 2004.

[31] T. E. Tezduyar and S. Sathe. Enhanced-discretization space-time technique (EDSTT). *Computer Methods in Applied Mechanics and Engineering*, 193:1385–1401, 2004.

[32] T.E. Tezduyar. Computation of moving boundaries and interfaces and stabilization parameters. *International Journal of Numerical Methods in Fluids*, 43:555–575, 2003.

[33] T.E. Tezduyar. Finite elements in fluids: Stabilized formulations and moving boundaries and interfaces. *Computers and Fluids*, 36:191–206, 2007.

[34] T.E. Tezduyar and M. Senga. Stabilization and shock-capturing parameters in SUPG formulation of compressible flows. *Computer Methods in Applied Mechanics and Engineering*, 195:1621–1632, 2006.

[35] T.E. Tezduyar and M. Senga. SUPG finite element computation of inviscid supersonic flows with YZβ shock-capturing. *Computers and Fluids*, 36:147–159, 2007.

[36] T.E. Tezduyar, M. Senga, and D. Vicker. Computation of inviscid supersonic flows around cylinders and spheres with the SUPG formulation and YZβ shock-capturing. *Computational Mechanics*, 38:469–481, 2006.

[37] Y. Zhang, Y. Bazilevs, S. Goswami, C. Bajaj, and T. J. R. Hughes. Patient-specific vascular NURBS modeling for isogeometric analysis of blood flow. *Computer Methods in Applied Mechanics and Engineering*, 2006. Submitted.

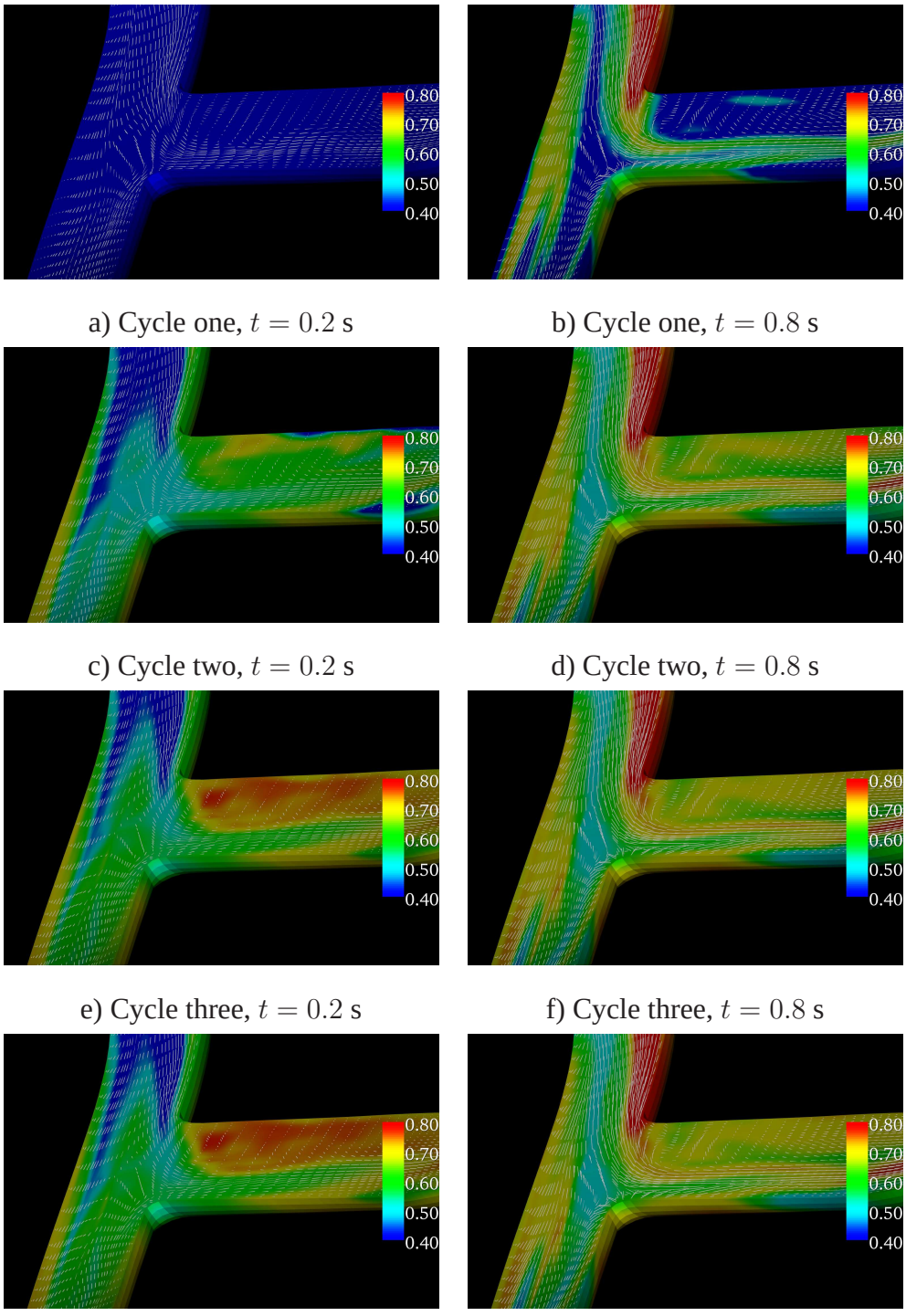

a) Cycle one, $t = 0.2$ s

b) Cycle one, $t = 0.8$ s

c) Cycle two, $t = 0.2$ s

d) Cycle two, $t = 0.8$ s

e) Cycle three, $t = 0.2$ s

f) Cycle three, $t = 0.8$ s

g) Cycle four, $t = 0.2$ s

h) Cycle four, $t = 0.8$ s

Fig. 10. Patient-specific modeling of drug delivery in coronary arteries. Blood flow velocity vectors superimposed on the drug concentration value at the arterial branching. Note the high concentration of drug in the recirculation zone. Also note that the differences between the third and fourth heartbeat cycles are minor, suggesting that a nearly time-periodic solution is achieved.